

Amplified emission and lasing in a plasmonic nanolaser with many three-level molecules

Yuan Zhang* and Klaus Mølmer†

Department of Physics and Astronomy, Aarhus University, Ny Munkegade 120, DK-8000 Aarhus C, Denmark (Received 20 November 2017; published 24 January 2018)

Steady-state plasmonic lasing is studied theoretically for a system consisting of many dye molecules arranged regularly around a gold nanosphere. A three-level model with realistic molecular dissipation is employed to analyze the performance as a function of the pump field amplitude and number of molecules. Few molecules and moderate pumping produce a single narrow emission peak because the excited molecules transfer energy to a single dipole plasmon mode by amplified spontaneous emission. Under strong pumping, the single peak splits into broader and weaker emission peaks because two molecular excited levels interfere with each other through coherent coupling with the pump field and with the dipole plasmon field. A large number of molecules gives rise to a Poisson-like distribution of plasmon number states with a large mean number characteristic of lasing action. These characteristics of lasing, however, deteriorate under strong pumping because of the molecular interference effect.

DOI: [10.1103/PhysRevA.97.013837](https://doi.org/10.1103/PhysRevA.97.013837)**I. INTRODUCTION**

The prospects of observing quantum effects in the response of metallic material to light [1] and exploring their potential applications [2–4] have stimulated abundant recent studies in plasmonics. Most of the envisioned applications are based on the enhanced and localized electromagnetic (EM) field near metallic films and nanoparticles (MNP), due to the formation of surface plasmons, i.e., collective oscillations of the EM field and the conduction electrons in the metal. This enhancement leads to strong light-matter interaction and enhanced absorption [5,6], emission [7], and Raman scattering [8,9] of quantum emitters, which can be naturally utilized to improve sensitivity of spectroscopic instruments [10,11] and efficiency of light emitting diodes [12,13] and solar cells [14,15]. Plasmon field modes, confined within subwavelength volumes, were utilized by Bergman and Stockman [16] to propose the “spaser” or plasmonic nanolaser in 2003, which was then verified in experiments by Noginov and his co-workers in 2009 [17] with a system consisting of a gold nanosphere and many dye molecules. Later experimental demonstrations of the spaser have been reported with structures like semiconductor wires [18–20] and squares [21,22] on metallic films, with semiconductor pillars [23,24], dots [25,26], and wires [27,28] inside metallic shells and with dye molecules deposited in periodically arranged MNP arrays [29–33].

Semiclassical theories based on rate equations [16,25–27] and Maxwell-Bloch equations [30–32] have been utilized to study the plasmonic nanolaser. These equations can incorporate coherent molecular excitation mechanisms and inhomogeneous coupling and multiple lasing modes, but they ignore quantum correlations between the molecules and the lasing modes. While quantum theories accounting for these

correlations have been presented with plasmon number states [34] or coherent states [35], the molecules have been always considered as identical two-level systems and the pumping mechanism has been simply modeled with an incoherent pumping rate.

To model the real and coherent pumping mechanism more realistically and understand its influence on the system quantum properties, we develop a quantum laser theory for the system shown in Fig. 1(a) (resembling the one in the experiment [17]). We thus consider the molecules as identical three-level systems, where one molecular transition couples with an external optical (driving) field and another transition couples with the plasmon lasing mode. Remarkably, we find that the two molecular excited states can interfere with each other due to the two couplings, which leads to emission peak splitting and reduced emission intensity.

The article is outlined as follows. In Sec. II, we introduce a master equation to describe the dynamics of many molecules and a single quantized plasmon mode. In Sec. III, we solve this equation with an exact numerical method based on a collective reduced density matrix (RDM), which applies to systems with identical molecules. In Sec. IV, we apply an approximate method, more general than Lamb’s laser theory [36], based on elimination of the molecular degrees of freedom and solution of a plasmon master equation. This method is verified and subsequently used to simulate systems with hundreds of molecules. In Sec. V, we conclude and discuss possible extensions of our theory.

II. MASTER EQUATION

We assume the molecules located around the equator of the sphere at a distance of 2.5 nm from the surface, see Fig. 1, which is sufficient to exclude tunneling ionization [37]. The molecules thus only exchange energy with the sphere through the dipole plasmon mode, which is resonant with the molecules and has its transition dipole moment along the z axis. The more

*y Zhang@phys.au.dk

†moelmer@phys.au.dk

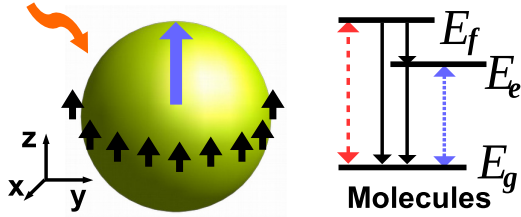


FIG. 1. A gold nanosphere (10 nm radius) is surrounded by dye molecules along the equator about 2.5 nm from the sphere surface. The molecules have transition dipole moments along the z axis (black arrows) and couple only with the dipole plasmon z mode (blue arrow). The molecules are assumed identical with three energy levels (E_g , E_e , E_f), and are coupled coherently to an external optical pump field (red dashed arrow) and to the dipole plasmon (blue dotted arrows), and decay by dissipation (black arrows).

general configuration involving randomly oriented molecules and three resonant dipole plasmons has been investigated in [38]. Higher multipole plasmons are off resonant and do not affect the molecules [39] apart from a contribution to their excited-state decay [40].

The master equation for the density operator $\hat{\rho}$ of the plasmon mode and the molecular emitters reads

$$\frac{\partial}{\partial t} \hat{\rho} = -\frac{i}{\hbar} [H_{\text{pl}} + H_{\text{m}} + V_{\text{pl-m}} + V_{\text{m}}(t), \hat{\rho}] - \mathcal{D}[\hat{\rho}]. \quad (1)$$

The plasmon mode with excitation energy $\hbar\omega_{\text{pl}}$ is described by the Hamiltonian $H_{\text{pl}} = \hbar\omega_{\text{pl}} C^{\dagger} C$ with bosonic creation and annihilation operators C^{\dagger} , C . The Hamiltonian of N_{m} molecules reads $H_{\text{m}} = \sum_{n=1}^{N_{\text{m}}} \sum_{a_n} E_{a_n} |a_n\rangle \langle a_n|$, with the single molecular ground state $|a_n = g_n\rangle$, and first $|a_n = e_n\rangle$ and second $|a_n = f_n\rangle$ excited states with energies E_{g_n} , E_{e_n} , and E_{f_n} , respectively. We assume that the plasmon mode couples resonantly with the molecular ground-to-first excited-state transition through the interaction Hamiltonian $V_{\text{pl-m}} = \hbar \sum_{n=1}^{N_{\text{m}}} v_{ge}^{(n)} (C^{\dagger} |g_n\rangle \langle e_n| + \text{H.c.})$ (in the rotating wave approximation). Here, the coefficient $\hbar v_{ge}^{(n)} = [\mathbf{d}_{ge}^{(n)} \cdot \mathbf{d}_{\text{pl}} - 3(\mathbf{d}_{ge}^{(n)} \cdot \hat{\mathbf{x}}_n)(\mathbf{d}_{\text{pl}} \cdot \hat{\mathbf{x}}_n)]/|\mathbf{X}_n|^3$ is determined by molecular and plasmon transition dipole moments $\mathbf{d}_{ge}^{(n)}$, and $\mathbf{d}_{\text{pl}} = d_{\text{pl}} \mathbf{e}_z$ (\mathbf{e}_z is the unit vector along the z axis), and by the vectors $\mathbf{X}_n = X_n \hat{\mathbf{x}}_n$, connecting the molecules and the sphere center. We assume that the molecules are subject to a driving field with frequency ω_0 , resonant with the molecular ground-to-second excited-state transition through the Hamiltonian $V_{\text{m}}(t) = \hbar \sum_{n=1}^{N_{\text{m}}} v_{gf}^{(n)} (e^{i\omega_0 t} |g_n\rangle \langle f_n| + \text{H.c.})$, where $\hbar v_{gf}^{(n)} = \mathbf{d}_{gf}^{(n)} \cdot \mathbf{n} E_0$ is determined by the molecular transition dipole moment $\mathbf{d}_{gf}^{(n)}$ and the driving field amplitude E_0 and polarization \mathbf{n} . Dissipation is accounted for by several Lindblad terms:

$$\mathcal{D}[\hat{\rho}] = (1/2) \sum_u k_u ([\hat{L}_u^{\dagger} \hat{L}_u, \hat{\rho}]_+ - 2\hat{L}_u \hat{\rho} \hat{L}_u^{\dagger}). \quad (2)$$

Plasmon damping is included by terms with $k_u = \gamma_{\text{pl}}$ and $\hat{L}_u = C$. γ_{pl} is mainly caused by electron-phonon collisions, while for small metallic particles as considered here the electron-surface collisions and radiation damping also contribute to the value of γ_{pl} [41]. The decay processes in the individual molecules are represented by terms with $k_u = k_{a \rightarrow b}^{(n)}$ and $\hat{L}_u = |b_n\rangle \langle a_n|$

for $E_{a_n} > E_{b_n}$. For simplicity, we ignore pure dephasing of the molecules.

III. COLLECTIVE REDUCED DENSITY MATRIX EQUATION

Due to symmetry, the density matrix must at all times be invariant under permutation of the identical molecules. For two-level systems, this is utilized in collective representations of the density matrix with Dicke states [42,43], SU(4) group theory [44], and collective numbers [34,45]. Here, we choose the latter representation since it can be easily extended to systems with multilevel molecules [46,47]. We consider the density matrix element $\rho_{\beta\nu,\alpha\mu}(t)$ between plasmon number states $|\mu\rangle$ and $|\nu\rangle$ and molecular product states $|\alpha\rangle \equiv \prod_{n=1}^{N_{\text{m}}} |a_n\rangle$ and $|\beta\rangle \equiv \prod_{n=1}^{N_{\text{m}}} |b_n\rangle$. The invariance under permutation of the molecules permits the representation of many of these matrix elements by one and the same number that we denote by $\rho_{\mathbf{n}}^{\mu\nu}$ where $\mathbf{n} = \{n_{ab}\}$ counts the number of occurrences of $|a_n = a\rangle$ and $|b_n = b\rangle$ in the states $|\alpha\rangle$ and $|\beta\rangle$. The master equation couples different matrix elements which can be all systematically represented in the reduced form. We effectively obtain a significantly reduced set of coupled equations for the collective RDM $\rho_{\mathbf{n}}^{\mu\nu}$. The resulting equations are presented as Eq. (B1) in Appendix B. The number $C_{N_{\text{m}}+8}^8 (N_{\text{pl}} + 1)^2$ of $\rho_{\mathbf{n}}^{\mu\nu}$ is order of magnitudes smaller than the number $[3^{N_{\text{m}}}(N_{\text{pl}} + 1)]^2$ of $\rho_{\beta\nu,\alpha\mu}$. Here, N_{pl} indicates the highest plasmon state considered. For example, for a system with ten molecules and six plasmon states, we reduce the number of elements from 1.3×10^{11} to 1.6×10^6 . For more details of the method please refer to our article [48] about the collective density matrix of multilevel emitters.

Using the density matrix with elements $\rho_{\mathbf{n}}^{\mu\nu} \equiv \rho_{\beta\nu,\alpha\mu}$, we can calculate all physical observables, for example, the population of the molecular states $|a = a_n\rangle$: P_a (a for g, e, f), the plasmon number state distribution $|\mu\rangle$: $P_{\mu} = \sum_{\alpha} P_{\alpha\mu}$, and the mean plasmon number $A_{\text{pl}} = \sum_{\mu} \mu P_{\mu}$ as well as its normalized second factorial moment $g_{\text{pl}}^2(0) = \sum_{\mu} \mu(\mu - 1) P_{\mu} / A_{\text{pl}}^2$ (this number characterizes the number distribution and equals unity for a coherent state). We can also apply the quantum regression theorem [49] and use the master equation to calculate two-time correlation functions and, e.g., the emission spectrum. The explicit expressions to compute these observables are detailed in Appendix B.

A. Exact numerical results for systems with up to ten molecules

Figure 2 shows the influence of strength of the driving field E_0 [Figs. 2(a)–2(c)] and decay rate $k_{f \rightarrow e}$ [Figs. 2(d)–2(f)] on the steady-state properties of systems with eight molecules. In the Fig. 2(a) the emission spectrum is weak for a weak driving field and it develops a sharp peak for moderate driving due to amplified spontaneous emission, which is verified by the increased population of the plasmon excited states [see Fig. 2(b)] and the molecular excited state [see the blue dotted line in Fig. 2(c)]. At strong driving, the spectrum becomes broadened and weak as a consequence of quantum interference between the two molecular excited states. Although these states do not directly couple with each other, they are coupled through the coherent coupling with the driving field and with

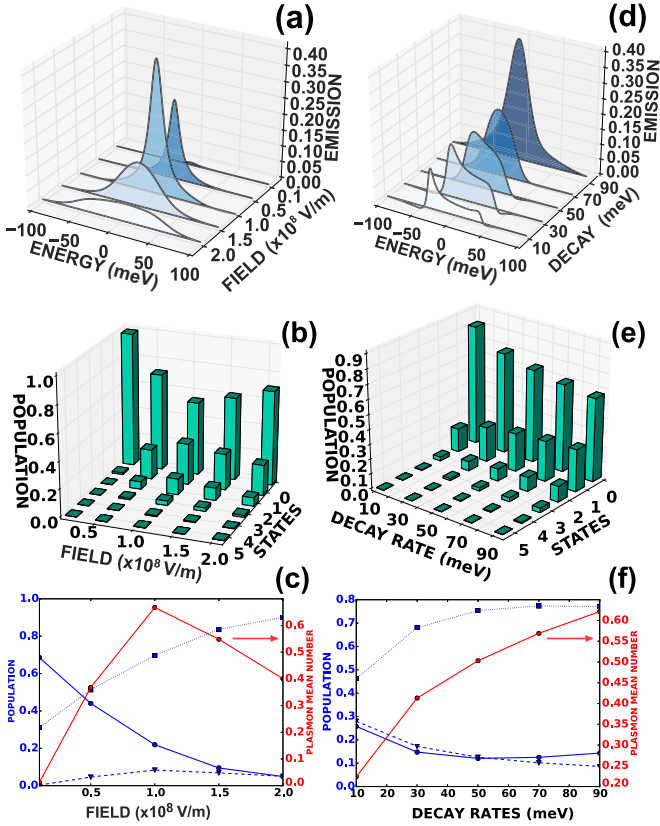


FIG. 2. Steady-state properties of systems with eight molecules for different strengths of the driving field E_0 [in panels (a)–(c)] and different decay rates $k_{f \rightarrow e}$ [in panels (d)–(f)]. Panels (a) and (d) give emission spectra (the photon energy is given relative to $\hbar\omega_{\text{pl}}$). Panels (b) and (e) give plasmon state populations P_μ . Panels (c) and (f) show molecular state populations P_a (blue lines; solid line P_g , dotted line P_e , dashed line P_f) and mean plasmon numbers A_{pl} . All further parameters are specified in Table I in Appendix A.

the plasmon mode, and a similar phenomenon occurs in the context of lasing without inversion [50]. If the fields couple to two separate transitions as in the four-level molecular model studied in [30], this interference effect is absent, and the emission intensity saturates but it does not deteriorate for large E_0 . Similar behavior of the mean plasmon number A_{pl} is observed [see the red line in Fig. 2(c)].

In Fig. 2(d), the emission spectrum shows two peaks, a broad peak and a single sharp peak with a broad background, for small, moderate, and large decay rates, respectively. In the absence of $k_{f \rightarrow e}$, the collective strong coupling of many molecules with the plasmon $\sqrt{N_m}v_{ge}$ (originating from $V_{\text{pl}-m}$ in the case of weak molecular excitation) leads to the formation of two dressed excited states with energies $E_\pm = \pm\sqrt{N_m}\hbar v_{ge}$ (relative to the plasmon energy $\hbar\omega_{\text{pl}}$) in the resonant case, i.e., $E_e - E_g = \hbar\omega_{\text{pl}}$. With $N_m = 8$ and $\hbar v_{ge} = 14$ meV this yields $E_\pm \approx \pm 40$ meV and explains the double peak splitting. The population of the dressed states is governed by the quantum interference between the molecular excited states. In the presence of $k_{f \rightarrow e}$, the population is in favor of the state with higher energy and this explains the asymmetry of the two peak intensities. For large value of $k_{f \rightarrow e}$, the interference is suppressed and the single sharp peak results

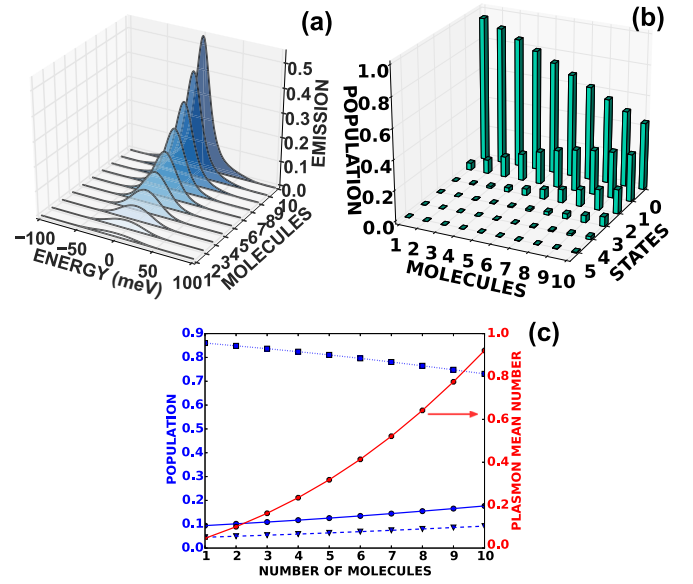


FIG. 3. Steady-state (a) emission spectrum (the photon energy is given relative to $\hbar\omega_{\text{pl}}$), (b) plasmon number state distribution P_μ , and (c) molecular state population P_a (blue lines: solid line P_g , dotted line P_e , dashed line P_f) as well as mean plasmon number A_{pl} (red line) for different numbers of molecules. All further parameters are specified in Table I in Appendix A.

from amplified spontaneous emission. The emission intensity increases with increasing $k_{f \rightarrow e}$ because the molecules with increasing population on the excited state P_e [see the dotted line in Fig. 2(f)] transfer more energy to the plasmon, which leads to increased population of the plasmon higher excited states [see Fig. 2(e)] and plasmon mean number [see the red line in Fig. 2(f)].

Figure 3 displays how the number of molecules N_m affects the emission and the plasmon state population P_μ , respectively. In Fig. 3(a) the emission shows higher intensity and spectral narrowing for the larger values of N_m . Figure 3(b) shows that only the $\mu = 0, 1$ plasmon number states are populated for $N_m = 1$. With increasing N_m , the plasmon states with $\mu \geq 1$ are gradually populated indicating an increased mean plasmon number [see the red line in Fig. 3(c)] and strong plasmon excitation. However, because of the backaction of the strong plasmon excitation, the population of molecular excited state P_e reduces [see the dotted blue line in Fig. 3(c)]. These results clearly indicate a transition from fluorescence to amplified spontaneous emission. In the following section we shall demonstrate a further increase of the plasmon excitation, i.e., lasing action, for systems with more molecules.

IV. APPROXIMATE PLASMON RDM EQUATION

The collective RDM allows only simulation of systems with up to ten molecules because of the huge number of matrix elements and thus it is necessary to develop approximate methods to solve Eq. (1) for larger systems. Here we follow the same methods as have been applied to the laser [36,51] to adiabatically eliminate the molecular degree of freedom and derive equations only for the plasmon RDM $\rho_{\mu\nu} \equiv \text{tr}_S\{\hat{\rho}(t)|\nu\rangle\langle\mu|\}$. The detailed derivation is given in Appendix C.

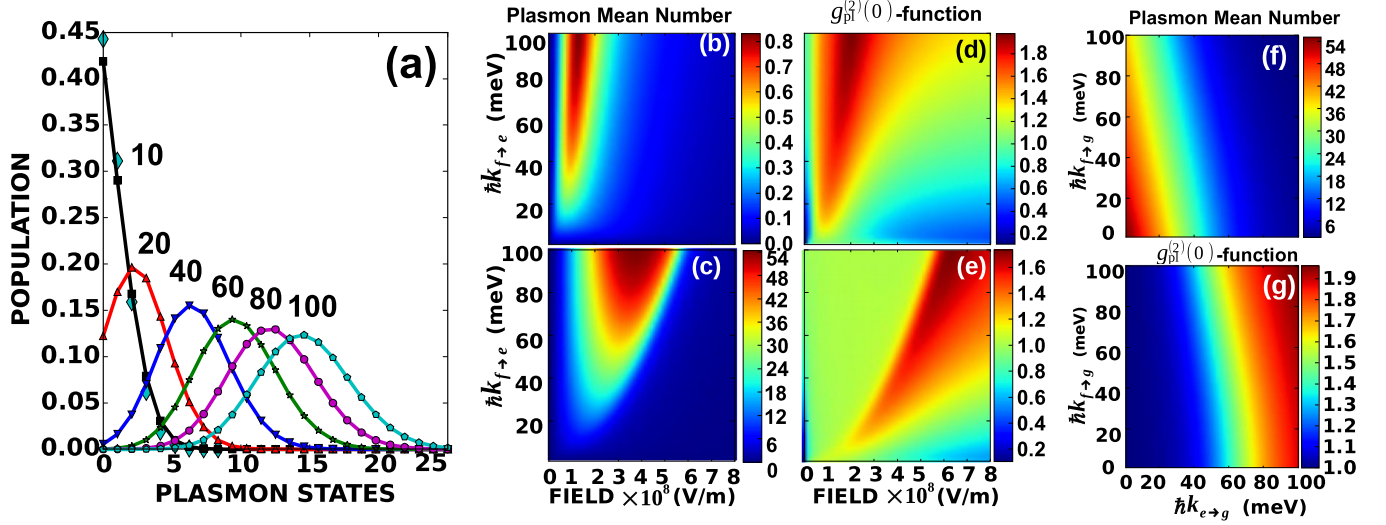


FIG. 4. Steady-state properties of systems: panel (a) calculated by Eq. (3) shows P_μ for different number of molecules, large diamonds show the exact result for ten molecules; panels (b) and (c) show A_{pl} and panels (d) and (e) show $g_{\text{pl}}^{(2)}(0)$ vs the decay rate $k_{f \rightarrow e}$ and the strength of the driving field E_0 ; panels (b) and (d) are for systems with 10 molecules; (c) and (e) are for systems with 200 molecules; panel (f) shows A_{pl} and (g) shows $g_{\text{pl}}^{(2)}(0)$ vs decay rates $k_{e \rightarrow g}$ and $k_{f \rightarrow g}$ for systems with 200 molecules ($\hbar k_{f \rightarrow e} = 100$ meV and $E_0 = 3 \times 10^8$ V/m). Other parameters are according to Table I in Appendix A.

Here we only outline the main procedure and present the final results.

Due to the molecule-plasmon coupling, the elements $\rho_{\mu\nu}$ depend on the values of the molecule-plasmon correlations $\rho_{e\mu-1,gv}^{(n)}$ and $\rho_{g\mu+1,ev}^{(n)}$, which are, in turn, coupled to the correlations $\tilde{\rho}_{f\mu,gv}^{(n)} \equiv e^{i\omega_0 t} \rho_{f\mu,gv}^{(n)}$ and $\tilde{\rho}_{f\mu,ev-1}^{(n)} \equiv e^{i\omega_0 t} \rho_{f\mu,ev-1}^{(n)}$, due to the simultaneous coupling with the plasmon and driving fields. Since the dissipation of both the molecules and the plasmon contributes to the decay of $\rho_{a\mu,b\nu}^{(n)}$, they should reach steady state much faster than the reduced elements $\rho_{\mu\nu}$, that evolve mainly by the plasmon decay rate. Thus, we apply an adiabatic elimination by assuming the steady-state solution for $\rho_{a\mu,b\nu}^{(n)}$. Similarly, correlations $\rho_{e\mu,ev}^{(n)}$, $\rho_{g\mu-1,gv-1}^{(n)}$, and $\rho_{f\mu-1,fv-1}^{(n)}$ can be expressed as combinations of $\rho_{e\mu-1,gv}^{(n)}$ and $\rho_{g\mu+1,ev}^{(n)}$ and $\rho_{\mu\nu}$, leading eventually to a closed set of equations for the plasmon RDM, see Eq. (C57) in Appendix C. It turns out that we obtain separate equations for the diagonal and off-diagonal elements, and we focus here on the plasmon state populations $P_\mu = \rho_{\mu\mu}$, obeying

$$\begin{aligned} \frac{\partial}{\partial t} P_\mu &= -[(\gamma_{\text{pl}}\mu + k_\mu)P_\mu - p_\mu P_{\mu-1}] \\ &\quad + [\gamma_{\text{pl}}(\mu + 1) + k_{\mu+1}]P_{\mu+1} - p_{\mu+1}P_\mu. \end{aligned} \quad (3)$$

TABLE I. Parameters used (for explanation see text).

$\hbar\omega_{\text{pl}}$	2.6 eV	$\hbar\omega_{eg}^{(n)}$	2.6 eV
$\hbar\gamma_{\text{pl}}$	100 meV	$\hbar\omega_{fg}^{(n)}$	2.7 eV
d_{pl}	2925 D	$d_{gf}^{(n)}$	16 D
$\Delta x_{\text{mol-MNP}}$	2.5 nm	$d_{ge}^{(n)}$	14.4 D
E_0	$0 \dots 10^9$ (1.2×10^8) V/m	$\hbar k_{f \rightarrow e}^{(n)}$	$0 \dots 100$ (100) meV
$\hbar\omega_0$	2.7 eV	Others	0 meV

The effective rates k_μ and p_μ are defined by Eqs. (C58) and (C59) in Appendix C and they can be viewed as extended Einstein A and B coefficients due to the molecular pumping mechanism. The rate k_μ describes loss of plasmons toward molecular excitation, and causes depopulation of higher excited plasmon states and increased population of lower excited plasmon states. The rate p_μ describes the plasmon emission by the excited molecules.

In steady state, the time derivatives in Eq. (3) vanish, and we obtain a recursion relation for the populations

$$r_\mu = P_\mu / P_{\mu-1} = p_\mu / (\gamma_{\text{pl}}\mu + k_\mu). \quad (4)$$

Together with the normalization $\sum_\mu P_\mu = 1$, this relation allows us to readily calculate P_μ for systems with hundreds and even thousands of molecules.

A. Results for systems with hundreds of molecules

The recursion relation (4) reproduces very well all the exact results shown in Fig. 3(b) and thus proves the validity of the adiabatic elimination of the molecular degrees of freedom in large systems. In this section we thus apply the reduced master equation (3) and thus Eq. (4) to systems with hundreds of molecules, see Fig. 4. Figure 4(a) shows the plasmon number distribution P_μ for systems with different numbers N_m of molecules. The big diamonds are the exact result for ten molecules and agree very well with the black squares calculated with Eq. (4). For $N_m = 10$ and 20, P_μ decreases with increasing μ , while for $N_m \geq 40$, the population distributions show a peak structure, shifting to higher plasmon excitation with increasing N_m . The Poisson-like distributions indicate lasing action, associated with the formation of a coherent state.

The variation of A_{pl} and $g_{\text{pl}}^{(2)}(0)$ is shown as a function of the driving field E_0 and the molecular dissipation rate $k_{f \rightarrow e}$ for systems with $N_m = 10$ molecules in Figs. 4(b) and 4(d) and

$N_m = 200$ in Figs. 4(c) and 4(e). Note the different plasmon number color bars in Figs. 4(b) and 4(c). The smaller systems show amplified spontaneous emission and their statistics are close to thermal, $g_{\text{pl}}^{(2)}(0) \approx 2$, see Fig. 4(d), when the plasmons are excited. The larger systems show lasing action with a large mean plasmon number $A_{\text{pl}} \gg 1$, and a Poisson-like distribution with $g_{\text{pl}}^{(2)}(0) = 1$ [see Fig. 4(e)].

Figures 4(f) and 4(g) illustrate the influence of the decay rates $k_{f \rightarrow g}, k_{e \rightarrow g}$ for systems with 200 molecules ($E_0 = 3 \times 10^8$ V/m and $\hbar k_{f \rightarrow e} = 100$ meV). Figure 4(f) shows that the increased decay rates reduce A_{pl} . This occurs because they reduce the population inversion $P_e - P_g$ and because $k_{e \rightarrow g}$ contributes to the molecular dephasing rate $\gamma_{ge}^{(n)}$. Figure 4(g) shows that regimes of high (low) plasmon numbers are governed by Poissonian (super Poissonian) statistics.

V. DISCUSSION AND OUTLOOK

In summary, we have solved the master equation for a plasmonic nanolaser with three-level molecules under continuous

optical pumping. We developed and applied an exact method for small systems with up to ten molecules and an approximate method for larger systems with hundreds of molecules. The small systems show amplified spontaneous emission, indicated by an increased emission intensity, but predominant population of lower plasmon number states and thermal-like statistics. The systems show a destructive quantum interference effect for strong pumping, leading to a reduced emission intensity and a split emission spectrum. The larger systems show lasing action as witnessed by a population of higher plasmon number states and Poisson-like statistics. The exact method can be generalized to systems with identical multilevel emitters [48] and is thus ideal to explore collective effects in those systems, for example, collective strong coupling and superradiance.

ACKNOWLEDGMENTS

The authors acknowledge C. Yu and L.F. Buchmann for several illuminating discussions. Their work was supported by the Villum Foundation.

APPENDIX A: SYSTEM PARAMETERS

In Table I, we collect the reference parameters for our simulations. We consider a gold nanosphere of 10 nm radius. For such a nanosphere, there are three dipole plasmons with transition dipole moments along three axes of the Cartesian coordinate system. They have the same excitation energy $\hbar\omega_{\text{pl}} = 2.6$ eV and damping rate $\hbar\gamma_{\text{pl}} = 100$ meV as well as a transition dipole moment $d_{\text{pl}} = 2925$ D. The driving field has an energy of $\hbar\omega_0 = 2.7$ eV and varying strength E_0 from 0 to 10^9 V/m. The molecules are assumed to be identical and have transition energy $\hbar\omega_{eg}^{(n)} = E_{e_n} - E_{g_n} = 2.6$ eV and transition dipole moments $d_{gf}^{(n)} = 16$ D and $d_{ge}^{(n)} = 14.4$ D. Here, we choose the transition energy $\hbar\omega_{fg}^{(n)} = E_{f_n} - E_{g_n} = 2.7$ eV to avoid resonant energy transfer to higher multipole plasmons. The decay rate $\hbar k_{f \rightarrow e}$ is varied from 0 to 100 meV while the other rates are zero. When the parameters are varied in the main text, we state their values in the figure legend.

The amplitude of the driving field E_0 is related to power density P by the relation $P = E^2/Z_0$ where $Z_0 \approx 377 \Omega$ is characteristic impedance of vacuum. When E_0 increases from $10^6, 10^7, 10^8$ to 10^9 V/m, P increases from 264 kW/cm², 26.4 MW/cm², 2.64×10^3 MW/cm² to 2.65×10^5 MW/cm². These values are consistent with the values used in the experiments [18,21,22,31–33].

APPENDIX B: COLLECTIVE REDUCED DENSITY MATRIX, POPULATION, AND EMISSION SPECTRUM

$$\begin{aligned} \frac{\partial}{\partial t} \rho_{\mathbf{n}}^{\mu\nu} = & -i(\mu - \nu)\omega_{\text{pl}}\rho_{\mathbf{n}}^{\mu\nu} - (\gamma_{\text{pl}}/2)[(\mu + \nu)\rho_{\mathbf{n}}^{\mu\nu} - 2\sqrt{(\mu + 1)(\nu + 1)}\rho_{\mathbf{n}}^{\mu+1\nu+1}] \\ & - i \sum_{a \neq b} \omega_{ba} n_{ab} \rho_{\mathbf{n}}^{\mu\nu} - \sum_{a \neq b} (k_{a \rightarrow b}/2) \left(\sum_c (n_{ac} + n_{ca}) \rho_{\mathbf{n}}^{\mu\nu} - 2n_{aa} \rho_{(n_{aa}-1, n_{bb}+1)}^{\mu\nu} \right) \\ & + i v_{ge} \sum_{a=g,e,f} [n_{ag} \sqrt{\nu} \rho_{(n_{ag}-1, n_{ae}+1)}^{\mu\nu-1} - n_{ea} \sqrt{\mu+1} \rho_{(n_{ea}-1, n_{ga}+1)}^{\mu+1\nu} + n_{ae} \sqrt{\nu+1} \rho_{(n_{ae}-1, n_{ag}+1)}^{\mu\nu+1} - \sqrt{\mu} n_{ga} \rho_{(n_{ga}-1, n_{ea}+1)}^{\mu-1\nu}] \\ & + i v_{gf} \sum_{a=g,e,f} [e^{i\omega_0 t} (n_{af} \rho_{(n_{af}-1, n_{ag}+1)}^{\mu\nu} - n_{ga} \rho_{(n_{ga}-1, n_{fa}+1)}^{\mu\nu}) + e^{-i\omega_0 t} (n_{ag} \rho_{(n_{ag}-1, n_{af}+1)}^{\mu\nu} - n_{fa} \rho_{(n_{fa}-1, n_{ga}+1)}^{\mu\nu})]. \quad (\text{B1}) \end{aligned}$$

In the main text, we have introduced the collective reduced density matrix (RDM) $\rho_{\mathbf{n}}^{\mu\nu}$ and explained the procedure to derive Eq. (B1) for such a matrix. More details can be found in [48]. In Eq. (B1) $\omega_{ba} = (E_{b_n} - E_{a_n})/\hbar$, $v_{ge} = v_{ge}^{(n)}$, and $v_{gf} = v_{gf}^{(n)}$. To abbreviate the notation, we indicate only the numbers that change, for example, $(n_{gg} - 1, n_{ee} + 1)$ represents \mathbf{n} ($\mathbf{n} = \{n_{ab}\}$) except n_{gg} is reduced by one and n_{ee} is increased by one.

In the following, we explain how to calculate the population and the emission spectrum from the collective RDM. The population of the system states $|\alpha\mu\rangle$ can be calculated by $P_{(n_{gg}, n_{ee}, n_{ff})}^{\mu} \equiv \rho_{(n_{gg}, 0, 0, 0, n_{ee}, 0, 0, 0, n_{ff})}^{\mu\mu}$ with n_{aa} being the number of molecules on the states $|a_n\rangle$. The population of the molecular product states $|\alpha\rangle$ is $P_{(n_{gg}, n_{ee}, n_{ff})}^{\mu} = \sum_{\mu} P_{(n_{gg}, n_{ee}, n_{ff})}^{\mu}$. The state population of individual

molecules $P_a = P_{a_n}$ can be calculated with

$$P_g = \sum_{n_{gg}=1}^{N_m} \sum_{n_{ee}=0}^{N_m-n_{gg}} C_{N_m-1}^{n_{gg}-1} C_{N_m-n_{gg}}^{n_{ee}} P_{(n_{gg}, n_{ee}, N_m-n_{gg}-n_{ee})}, \quad (\text{B2})$$

$$P_e = \sum_{n_{ee}=1}^{N_m} \sum_{n_{gg}=0}^{N_m-n_{ee}} C_{N_m-1}^{n_{ee}-1} C_{N_m-n_{ee}}^{n_{gg}} P_{(n_{gg}, n_{ee}, N_m-n_{gg}-n_{ee})}, \quad (\text{B3})$$

$$P_f = \sum_{n_{ff}=1}^{N_m} \sum_{n_{ee}=0}^{N_m-n_{ff}} C_{N_m-1}^{n_{ff}-1} C_{N_m-n_{ff}}^{n_{ee}} P_{(N_m-n_{ee}-n_{ff}, n_{ee}, n_{ff})}, \quad (\text{B4})$$

where $C_n^m = n!/[m!(n-m)!]$ is a combinational coefficient. The population of the plasmon states $|\mu\rangle$ can be calculated from

$$P_\mu = \sum_{n_{gg}=0}^{N_m} \sum_{n_{ee}=0}^{N_m-n_{gg}} C_{N_m}^{n_{gg}} C_{N_m-n_{gg}}^{n_{ee}} P_{(n_{gg}, n_{ee}, N_m-n_{gg}-n_{ee})}^\mu. \quad (\text{B5})$$

The average plasmon number $A_{\text{pl}} = \sum_\mu \mu P_\mu$ and the second-order correlation function at steady state $g_{\text{pl}}^2(0) = \sum_\mu \mu(\mu-1)P_\mu/A_{\text{pl}}^2$ can be directly calculated from P_μ .

The steady-state emission spectrum $F(\omega) \propto \text{Re} \int_0^\infty d\tau e^{-i\omega\tau} \langle C^+(\tau)C(0) \rangle$ is determined by the Fourier transformation of the correlation function $\langle C^+(\tau)C(0) \rangle$. According to the quantum regression theory [49], $\langle C^+(\tau)C(0) \rangle \equiv \text{tr}_s \{ C^+ \hat{\sigma}(\tau) \}$ can be calculated with the operator $\hat{\sigma}$ satisfying the same equation as $\hat{\rho}$ with, however, the initial condition $\hat{\sigma}(0) = C \hat{\rho}_{\text{ss}}$. Here, $\hat{\rho}_{\text{ss}}$ is the system reduced density operator at steady-state. For the identical molecules the steady-state emission spectrum becomes

$$F(\omega) \propto \text{Re} \int_0^\infty d\tau e^{-i\omega\tau} \sum_\mu \sqrt{\mu} \sum_{n_{ff}=0}^{N_m} \sum_{n_{ee}=0}^{N_m-n_{ff}} C_{N_m}^{n_{ff}} C_{N_m-n_{ff}}^{n_{ee}} \sigma_{(N_m-n_{ff}-n_{ee}, 0, 0, 0, n_{ee}, 0, 0, 0, n_{ff})}^{\mu-1\mu}(\tau). \quad (\text{B6})$$

The sigma matrix elements $\sigma_{\mathbf{n}}^{\mu, \nu}(\tau)$ satisfy the same equations as $\rho_{\mathbf{n}}^{\mu, \nu}$, cf. Eq. (B1), with, however, the initial condition $\sigma_{\mathbf{n}}^{\mu, \nu}(\tau=0) = \sqrt{\mu+1} \rho_{\mathbf{n}, \text{ss}}^{\mu+1, \nu}$ given by the steady-state collective RDM.

APPENDIX C: DERIVATION OF APPROXIMATE EQUATION FOR PLASMON RDM

Because of the computational effort involved in solving the collective RDM equation, we can only simulate systems with few molecules. To solve the Eq. (1) in the main text for many molecules, we have presented an approximate method based on the plasmon RDM $\rho_{\mu\nu} \equiv \text{tr}_S \{ \hat{\rho}(t) | \nu \rangle \langle \mu | \}$. The equation for this matrix can be easily derived from Eq. (1):

$$\begin{aligned} \frac{\partial}{\partial t} \rho_{\mu\nu} &= -i\omega_{\mu\nu} \rho_{\mu\nu} - \gamma_{\text{pl}} [(\mu+\nu)/2] \rho_{\mu\nu} + \gamma_{\text{pl}} \sqrt{(\mu+1)(\nu+1)} \rho_{\mu+1\nu+1} \\ &- \sum_{n=1}^{N_m} i v_{ge}^{(n)} (\sqrt{\mu} \rho_{e\mu-1, g\nu}^{(n)} - \sqrt{\nu} \rho_{g\mu, e\nu-1}^{(n)}) + \sum_{n=1}^{N_m} i v_{ge}^{(n)} (\sqrt{\nu+1} \rho_{e\mu, g\nu+1}^{(n)} - \sqrt{\mu+1} \rho_{g\mu+1, e\nu}^{(n)}). \end{aligned} \quad (\text{C1})$$

This equation depends on the molecule-plasmon correlations $\rho_{a\mu, b\nu}^{(n)}$. The equations for these correlations can be again derived from Eq. (1) in the main text. For the derivation, we introduce the following replacement

$$- [i\omega_{\mu\nu} - \gamma_{\text{pl}}(\mu+\nu)/2] \rho_{a\mu, b\nu}^{(n)} + \gamma_{\text{pl}} \sqrt{(\mu+1)(\nu+1)} \rho_{a\mu+1, b\nu+1}^{(n)} \rightarrow -i\tilde{\omega}_{\mu\nu} \rho_{a\mu, b\nu}^{(n)}. \quad (\text{C2})$$

This removes the dependence of higher plasmon excited states due to the plasmon damping without underestimating its influence. This has been successfully applied in our previous work on lasers with two-level [45] and three-level molecules [47], because the differences introduced by the replacement are very small if the higher number states are involved. Here, the complex transition frequency is defined as

$$\tilde{\omega}_{\mu\nu} = \omega_{\mu\nu} - i\gamma_{\text{pl}} [(\mu+\nu)/2 - \sqrt{\mu\nu}]. \quad (\text{C3})$$

Due to the coupling with the driving field, we can introduce the following slowly varying correlations $\tilde{\rho}_{f\mu, g\nu}^{(n)} \equiv e^{i\omega_0 t} \rho_{f\mu, g\nu}^{(n)}$, $\tilde{\rho}_{g\mu, f\nu}^{(n)} \equiv e^{-i\omega_0 t} \rho_{g\mu, f\nu}^{(n)}$, $\tilde{\rho}_{f\mu, e\nu-1}^{(n)} \equiv e^{i\omega_0 t} \rho_{f\mu, e\nu-1}^{(n)}$, and $\tilde{\rho}_{e\mu-1, f\nu}^{(n)} \equiv e^{-i\omega_0 t} \rho_{e\mu-1, f\nu}^{(n)}$. Finally, we get the equations for the correlations.

First, we present the equations for the population-like correlations $\rho_{a\mu, a\nu}^{(n)}$:

$$\begin{aligned} \frac{\partial}{\partial t} \rho_{g\mu, g\nu}^{(n)} &= -i\tilde{\omega}_{\mu\nu} \rho_{g\mu, g\nu}^{(n)} - (k_{g \rightarrow f}^{(n)} + k_{e \rightarrow f}^{(n)}) \rho_{g\mu, g\nu}^{(n)} + k_{f \rightarrow g}^{(n)} \rho_{f\mu, f\nu}^{(n)} + k_{e \rightarrow g}^{(n)} \rho_{e\mu, e\nu}^{(n)} \\ &+ i v_{ge}^{(n)} (\sqrt{\nu} \rho_{g\mu, e\nu-1}^{(n)} - \sqrt{\mu} \rho_{e\mu-1, g\nu}^{(n)}) - i v_{gf}^{(n)} (\tilde{\rho}_{f\mu, g\nu}^{(n)} - \tilde{\rho}_{g\mu, f\nu}^{(n)}), \end{aligned} \quad (\text{C4})$$

$$\frac{\partial}{\partial t} \rho_{e\mu-1, ev-1}^{(n)} = -i\tilde{\omega}_{\mu-1\nu-1} \rho_{e\mu-1, ev-1}^{(n)} + k_{g \rightarrow e}^{(n)} \rho_{g\mu-1, gv-1}^{(n)} + k_{f \rightarrow e}^{(n)} \rho_{f\mu-1, fv-1}^{(n)} - (k_{e \rightarrow g}^{(n)} + k_{e \rightarrow f}^{(n)}) \rho_{e\mu-1, ev-1}^{(n)} + i v_{ge}^{(n)} (\sqrt{\nu} \rho_{e\mu-1, gv}^{(n)} - \sqrt{\mu} \rho_{g\mu, ev-1}^{(n)}), \quad (C5)$$

$$\frac{\partial}{\partial t} \rho_{f\mu, fv}^{(n)} = -i\tilde{\omega}_{\mu\nu} \rho_{f\mu, fv}^{(n)} - (k_{f \rightarrow g}^{(n)} + k_{f \rightarrow e}^{(n)}) \rho_{f\mu, fv}^{(n)} + k_{g \rightarrow f}^{(n)} \rho_{g\mu, gv}^{(n)} + k_{e \rightarrow f}^{(n)} \rho_{e\mu, ev}^{(n)} + i v_{gf}^{(n)} (\tilde{\rho}_{f\mu, gv}^{(n)} - \tilde{\rho}_{g\mu, fv}^{(n)}). \quad (C6)$$

Obviously, these correlations couple with the coherence-like correlations $\rho_{a\mu, b\nu}^{(n)}$ with $a \neq b$. Their equations are

$$\frac{\partial}{\partial t} \rho_{g\mu, ev-1}^{(n)} = i(\tilde{\omega}_{eg}^{(n)*} - \tilde{\omega}_{\mu\nu-1}) \rho_{g\mu, ev-1}^{(n)} + i v_{ge}^{(n)} (\sqrt{\nu} \rho_{g\mu, gv}^{(n)} - \sqrt{\mu} \rho_{e\mu-1, ev-1}^{(n)}) - i v_{gf}^{(n)} \tilde{\rho}_{f\mu, ev-1}^{(n)}, \quad (C7)$$

$$\frac{\partial}{\partial t} \rho_{e\mu-1, gv}^{(n)} = -i(\tilde{\omega}_{eg}^{(n)} + \tilde{\omega}_{\mu-1\nu}) \rho_{e\mu-1, gv}^{(n)} + i v_{ge}^{(n)} (\sqrt{\nu} \rho_{e\mu-1, ev-1}^{(n)} - \sqrt{\mu} \rho_{g\mu, gv}^{(n)}) + i v_{gf}^{(n)} \rho_{e\mu-1, fv}^{(n)}, \quad (C8)$$

$$\frac{\partial}{\partial t} \tilde{\rho}_{e\mu-1, fv}^{(n)} = -i(\tilde{\omega}_{ef}^{(n)} + \tilde{\omega}_{\mu-1\nu}) \tilde{\rho}_{e\mu-1, fv}^{(n)} + i v_{gf}^{(n)} \rho_{e\mu-1, gv}^{(n)} - i v_{ge}^{(n)} \sqrt{\mu} \tilde{\rho}_{g\mu, fv}^{(n)}, \quad (C9)$$

$$\frac{\partial}{\partial t} \tilde{\rho}_{f\mu, ev-1}^{(n)} = i(\tilde{\omega}_{ef}^{(n)*} - \tilde{\omega}_{\mu\nu-1}) \tilde{\rho}_{f\mu, ev-1}^{(n)} - i v_{gf}^{(n)} \rho_{g\mu, ev-1}^{(n)} + i v_{ge}^{(n)} \sqrt{\nu} \tilde{\rho}_{f\mu, gv}^{(n)}, \quad (C10)$$

$$\frac{\partial}{\partial t} \tilde{\rho}_{g\mu, fv}^{(n)} = -i(\tilde{\omega}_{gf}^{(n)} + \tilde{\omega}_{\mu\nu}) \tilde{\rho}_{g\mu, fv}^{(n)} - i v_{ge}^{(n)} \sqrt{\mu} \tilde{\rho}_{e\mu-1, fv}^{(n)} + i v_{gf}^{(n)} (\rho_{g\mu, gv}^{(n)} - \rho_{f\mu, fv}^{(n)}), \quad (C11)$$

$$\frac{\partial}{\partial t} \tilde{\rho}_{f\mu, gv}^{(n)} = i(\tilde{\omega}_{gf}^{(n)*} - \tilde{\omega}_{\mu\nu}) \tilde{\rho}_{f\mu, gv}^{(n)} + i v_{ge}^{(n)} \sqrt{\nu} \tilde{\rho}_{f\mu, ev-1}^{(n)} - i v_{gf}^{(n)} (\rho_{g\mu, gv}^{(n)} - \rho_{f\mu, fv}^{(n)}). \quad (C12)$$

In the above expressions, we have also introduced complex transition frequencies $\tilde{\omega}_{eg}^{(n)} = \omega_{eg}^{(n)} - i\gamma_{eg}^{(n)}$ with the dephasing rate $\gamma_{eg}^{(n)} \equiv (k_{e \rightarrow g}^{(n)} + k_{e \rightarrow f}^{(n)} + k_{g \rightarrow e}^{(n)} + k_{g \rightarrow f}^{(n)})/2$, $\tilde{\omega}_{ef}^{(n)} = \omega_{ef}^{(n)} + \omega_0 - i\gamma_{ef}^{(n)}$ with $\gamma_{ef}^{(n)} \equiv (k_{e \rightarrow g}^{(n)} + k_{e \rightarrow f}^{(n)} + k_{f \rightarrow g}^{(n)} + k_{f \rightarrow e}^{(n)})/2$ and $\tilde{\omega}_{gf}^{(n)} = \omega_{gf}^{(n)} + \omega_0 - i\gamma_{gf}^{(n)}$ with $\gamma_{gf}^{(n)} \equiv (k_{g \rightarrow e}^{(n)} + k_{g \rightarrow f}^{(n)} + k_{f \rightarrow e}^{(n)} + k_{f \rightarrow g}^{(n)})/2$. If relevant, pure dephasing rates of the molecules can also be included in the above dephasing rates.

Following the procedure stated in the main text, we can get closed equations for the plasmon RDM. In practice, first, we express the steady-state coherence-like correlations $\rho_{a\mu, b\nu}^{(n)}$ ($a \neq b$) with the population-like correlations $\rho_{a\mu, a\nu}^{(n)}$. Second, we insert those expressions in the equations for the latter correlations and solve the closed equations analytically. Third, we utilize the expressions achieved to get analytical solutions for the correlations, which we insert into Eq. (C1) to get the equations for $\rho_{\mu\nu}$.

By setting the time derivatives to zero in Eqs. (C9) and (C10), we have

$$\tilde{\rho}_{e\mu-1, fv}^{(n)} = \frac{v_{gf}^{(n)} \rho_{e\mu-1, gv}^{(n)} - v_{ge}^{(n)} \sqrt{\mu} \tilde{\rho}_{g\mu, fv}^{(n)}}{\tilde{\omega}_{ef}^{(n)} + \tilde{\omega}_{\mu-1\nu}}, \quad (C13)$$

$$\tilde{\rho}_{f\mu, ev-1}^{(n)} = \frac{v_{gf}^{(n)} \rho_{g\mu, ev-1}^{(n)} - v_{ge}^{(n)} \sqrt{\nu} \tilde{\rho}_{f\mu, gv}^{(n)}}{\tilde{\omega}_{ef}^{(n)*} - \tilde{\omega}_{\mu\nu-1}}. \quad (C14)$$

From Eqs. (C11) and (C12) we get

$$\tilde{\rho}_{g\mu, fv}^{(n)} = \frac{v_{gf}^{(n)} (\rho_{g\mu, gv}^{(n)} - \rho_{f\mu, fv}^{(n)}) - v_{ge}^{(n)} \sqrt{\mu} \tilde{\rho}_{e\mu-1, fv}^{(n)}}{\tilde{\omega}_{gf}^{(n)} + \tilde{\omega}_{\mu\nu}}, \quad (C15)$$

$$\tilde{\rho}_{f\mu, gv}^{(n)} = \frac{v_{gf}^{(n)} (\rho_{g\mu, gv}^{(n)} - \rho_{f\mu, fv}^{(n)}) - v_{ge}^{(n)} \sqrt{\nu} \tilde{\rho}_{f\mu, ev-1}^{(n)}}{\tilde{\omega}_{gf}^{(n)*} - \tilde{\omega}_{\mu\nu}}. \quad (C16)$$

Inserting Eqs. (C13) and (C14) into Eqs. (C15) and (C16), we have

$$\tilde{\rho}_{g\mu, fv}^{(n)} = -\Xi_{\mu\nu}^{(n)} v_{gf}^{(n)} [v_{ge}^{(n)} \sqrt{\mu} \rho_{e\mu-1, gv}^{(n)} - (\tilde{\omega}_{ef}^{(n)} + \tilde{\omega}_{\mu-1\nu}) (\rho_{g\mu, gv}^{(n)} - \rho_{f\mu, fv}^{(n)})], \quad (C17)$$

$$\tilde{\rho}_{f\mu, gv}^{(n)} = -\tilde{\Xi}_{\mu\nu}^{(n)} v_{gf}^{(n)} [v_{ge}^{(n)} \sqrt{\nu} \rho_{g\mu, ev-1}^{(n)} - (\tilde{\omega}_{ef}^{(n)*} - \tilde{\omega}_{\mu\nu-1}) (\rho_{g\mu, gv}^{(n)} - \rho_{f\mu, fv}^{(n)})]. \quad (C18)$$

Here, we have introduced the abbreviations

$$1/\Xi_{\mu\nu}^{(n)} = (\tilde{\omega}_{ef}^{(n)} + \tilde{\omega}_{\mu-1\nu}) (\tilde{\omega}_{gf}^{(n)} + \tilde{\omega}_{\mu\nu}) - v_{ge}^{(n)2} \mu, \quad (C19)$$

$$1/\tilde{\Xi}_{\mu\nu}^{(n)} = (\tilde{\omega}_{ef}^{(n)*} - \tilde{\omega}_{\mu\nu-1}) (\tilde{\omega}_{gf}^{(n)*} - \tilde{\omega}_{\mu\nu}) - v_{ge}^{(n)2} \nu. \quad (C20)$$

We now insert Eqs. (C17) and (C18) into Eqs. (C4) and (C6) and obtain

$$i\tilde{\omega}_{\mu\nu}\rho_{g\mu,g\nu}^{(n)} = k_{f\rightarrow g}^{(n)}\rho_{f\mu,f\nu}^{(n)} + k_{e\rightarrow g}^{(n)}\rho_{e\mu,ev}^{(n)} + iv_{gf}^{(n)2}(\rho_{g\mu,g\nu}^{(n)} - \rho_{f\mu,f\nu}^{(n)})[\Xi_{\mu\nu}^{(n)}(\tilde{\omega}_{ef}^{(n)} + \tilde{\omega}_{\mu-1\nu}) - \tilde{\Xi}_{\mu\nu}^{(n)}(\tilde{\omega}_{ef}^{(n)*} - \tilde{\omega}_{\mu-1\nu})] \\ + iv_{ge}^{(n)}(1 + v_{gf}^{(n)2}\tilde{\Xi}_{\mu\nu}^{(n)})\sqrt{v}\rho_{g\mu,ev-1}^{(n)} - iv_{ge}^{(n)}(1 + v_{gf}^{(n)2}\Xi_{\mu\nu}^{(n)})\sqrt{\mu}\rho_{e\mu-1,g\nu}^{(n)}, \quad (\text{C21})$$

$$[i\tilde{\omega}_{\mu\nu} + k_{f\rightarrow g}^{(n)} + k_{f\rightarrow e}^{(n)}]\rho_{f\mu,f\nu}^{(n)} = k_{g\rightarrow f}^{(n)}\rho_{g\mu,g\nu}^{(n)} + k_{e\rightarrow f}^{(n)}\rho_{e\mu,ev}^{(n)} + iv_{gf}^{(n)2}[\tilde{\Xi}_{\mu\nu}^{(n)}(\tilde{\omega}_{ef}^{(n)*} - \tilde{\omega}_{\mu-1\nu}) - \Xi_{\mu\nu}^{(n)}(\tilde{\omega}_{ef}^{(n)} + \tilde{\omega}_{\mu-1\nu})] \\ \times (\rho_{g\mu,g\nu}^{(n)} - \rho_{f\mu,f\nu}^{(n)}) - iv_{gf}^{(n)2}\tilde{\Xi}_{\mu\nu}^{(n)}v_{ge}^{(n)}\sqrt{v}\rho_{g\mu,ev-1}^{(n)} + iv_{gf}^{(n)2}\Xi_{\mu\nu}^{(n)}v_{ge}^{(n)}\sqrt{\mu}\rho_{e\mu-1,g\nu}^{(n)}. \quad (\text{C22})$$

In addition, we also write down explicitly Eq. (C5) in steady state as

$$(i\tilde{\omega}_{\mu-1\nu-1} + k_{e\rightarrow g}^{(n)} + k_{e\rightarrow f}^{(n)})\rho_{e\mu-1,ev-1}^{(n)} = k_{g\rightarrow e}^{(n)}\rho_{g\mu-1,g\nu-1}^{(n)} + k_{f\rightarrow e}^{(n)}\rho_{f\mu-1,f\nu-1}^{(n)} + iv_{ge}^{(n)}(\sqrt{v}\rho_{e\mu-1,g\nu}^{(n)} - \sqrt{\mu}\rho_{g\mu,ev-1}^{(n)}). \quad (\text{C23})$$

Inserting Eqs. (C15) and (C16) into Eqs. (C13) and (C14), we have

$$\tilde{\rho}_{e\mu-1,f\nu}^{(n)} = \Xi_{\mu\nu}^{(n)}v_{gf}^{(n)}[(\tilde{\omega}_{gf}^{(n)} + \tilde{\omega}_{\mu\nu})\rho_{e\mu-1,g\nu}^{(n)} - v_{ge}^{(n)}\sqrt{\mu}(\rho_{g\mu,g\nu}^{(n)} - \rho_{f\mu,f\nu}^{(n)})], \quad (\text{C24})$$

$$\tilde{\rho}_{f\mu,ev-1}^{(n)} = \tilde{\Xi}_{\mu\nu}^{(n)}v_{gf}^{(n)}[(\tilde{\omega}_{gf}^{(n)*} - \tilde{\omega}_{\mu\nu})\rho_{g\mu,ev-1}^{(n)} - v_{ge}^{(n)}\sqrt{v}(\rho_{g\mu,g\nu}^{(n)} - \rho_{f\mu,f\nu}^{(n)})]. \quad (\text{C25})$$

Inserting the above results into Eqs. (C7) and (C8), we have

$$\rho_{g\mu,ev-1}^{(n)} = \tilde{\Phi}_{\mu\nu}^{(n)}\tilde{\Xi}_{\mu\nu}^{(n)}v_{gf}^{(n)2}v_{ge}^{(n)}\sqrt{v}(\rho_{g\mu,g\nu}^{(n)} - \rho_{f\mu,f\nu}^{(n)}) + \tilde{\Phi}_{\mu\nu}^{(n)}v_{ge}^{(n)}(\sqrt{v}\rho_{g\mu,g\nu}^{(n)} - \sqrt{\mu}\rho_{e\mu-1,ev-1}^{(n)}), \quad (\text{C26})$$

$$\rho_{e\mu-1,g\nu}^{(n)} = \Phi_{\mu\nu}^{(n)}\Xi_{\mu\nu}^{(n)}v_{gf}^{(n)2}v_{ge}^{(n)}\sqrt{\mu}(\rho_{g\mu,g\nu}^{(n)} - \rho_{f\mu,f\nu}^{(n)}) + \Phi_{\mu\nu}^{(n)}v_{ge}^{(n)}(\sqrt{\mu}\rho_{g\mu,g\nu}^{(n)} - \sqrt{v}\rho_{e\mu-1,ev-1}^{(n)}). \quad (\text{C27})$$

Here, we have introduced the abbreviations

$$1/\Phi_{\mu\nu}^{(n)} = \Xi_{\mu\nu}^{(n)}v_{gf}^{(n)2}(\tilde{\omega}_{gf}^{(n)} + \tilde{\omega}_{\mu\nu}) - (\tilde{\omega}_{eg}^{(n)} + \tilde{\omega}_{\mu-1\nu}), \quad (\text{C28})$$

$$1/\tilde{\Phi}_{\mu\nu}^{(n)} = \tilde{\Xi}_{\mu\nu}^{(n)}v_{gf}^{(n)2}(\tilde{\omega}_{gf}^{(n)*} - \tilde{\omega}_{\mu\nu}) - (\tilde{\omega}_{eg}^{(n)*} - \tilde{\omega}_{\mu-1\nu}). \quad (\text{C29})$$

Inserting Eqs. (C26) and (C27) into Eqs. (C21)–(C23), we get

$$\begin{bmatrix} M_{n;\mu\nu}^{(11)} & M_{n;\mu\nu}^{(12)} & M_{n;\mu\nu}^{(13)} \\ M_{n;\mu\nu}^{(21)} & M_{n;\mu\nu}^{(22)} & M_{n;\mu\nu}^{(23)} \\ M_{n;\mu\nu}^{(31)} & M_{n;\mu\nu}^{(32)} & M_{n;\mu\nu}^{(33)} \end{bmatrix} \begin{bmatrix} \rho_{g\mu,g\nu}^{(n)} \\ \rho_{e\mu-1,ev-1}^{(n)} \\ \rho_{f\mu,f\nu}^{(n)} \end{bmatrix} = \begin{bmatrix} k_{e\rightarrow g}^{(n)} \\ -k_{e\rightarrow f}^{(n)} \\ 0 \end{bmatrix} \rho_{\mu\nu} + \begin{bmatrix} 0 \\ 0 \\ -k_{f\rightarrow e}^{(n)} \end{bmatrix} \rho_{\mu-1\nu-1}. \quad (\text{C30})$$

Here, we have used $\rho_{e\mu,ev}^{(n)} = \rho_{\mu\nu} - \rho_{g\mu,g\nu}^{(n)} - \rho_{f\mu,f\nu}^{(n)}$ to get the first and second line of Eq. (C30). In order to get the third line of Eq. (C30), we replace $\rho_{f\mu-1,f\nu-1}^{(n)}$ by $\rho_{\mu-1,\nu-1}^{(n)} - \rho_{g\mu-1,g\nu-1}^{(n)} - \rho_{e\mu-1,ev-1}^{(n)}$ and then upgrade $\rho_{g\mu-1,g\nu-1}^{(n)}$ by $\rho_{g\mu,g\nu}^{(n)}$. The matrix elements $M_{n;\mu\nu}^{(ij)}$ are defined as follows:

$$M_{n;\mu\nu}^{(11)} = i\tilde{\omega}_{\mu\nu} + k_{e\rightarrow g}^{(n)} + A_{\mu\nu}^{(n)} + 2B_{\mu\nu}^{(n)} + C_{\mu\nu}^{(n)}, \quad (\text{C31})$$

$$M_{n;\mu\nu}^{(12)} = -(E_{\mu\nu}^{(n)} + F_{\mu\nu}^{(n)}), \quad (\text{C32})$$

$$M_{n;\mu\nu}^{(13)} = -(k_{f\rightarrow g}^{(n)} - k_{e\rightarrow g}^{(n)} + B_{\mu\nu}^{(n)} + C_{\mu\nu}^{(n)}), \quad (\text{C33})$$

$$M_{n;\mu\nu}^{(21)} = k_{g\rightarrow f}^{(n)} - k_{e\rightarrow f}^{(n)} + B_{\mu\nu}^{(n)} + C_{\mu\nu}^{(n)}, \quad (\text{C34})$$

$$M_{n;\mu\nu}^{(22)} = -F_{\mu\nu}^{(n)}, \quad (\text{C35})$$

$$M_{n;\mu\nu}^{(23)} = -(i\tilde{\omega}_{\mu\nu} + k_{f\rightarrow g}^{(n)} + k_{f\rightarrow e}^{(n)} + k_{e\rightarrow f}^{(n)} + C_{\mu\nu}^{(n)}), \quad (\text{C36})$$

$$M_{n;\mu\nu}^{(31)} = k_{g\rightarrow e}^{(n)} - k_{f\rightarrow e}^{(n)} + F_{\mu\nu}^{(n)} + E_{\mu\nu}^{(n)}, \quad (\text{C37})$$

$$M_{n;\mu\nu}^{(32)} = -(i\tilde{\omega}_{\mu-1\nu-1} + k_{e\rightarrow g}^{(n)} + k_{e\rightarrow f}^{(n)} + k_{f\rightarrow e}^{(n)} - G_{\mu\nu}^{(n)}), \quad (\text{C38})$$

$$M_{n;\mu\nu}^{(33)} = -F_{\mu\nu}^{(n)}. \quad (\text{C39})$$

Here, to simplify the expressions, we have introduced the abbreviations

$$A_{\mu\nu}^{(n)} = i v_{ge}^{(n)2} (\Phi_{\mu\nu}^{(n)} \mu - \tilde{\Phi}_{\mu\nu}^{(n)} \nu), \quad (\text{C40})$$

$$B_{\mu\nu}^{(n)} = i v_{gf}^{(n)2} v_{ge}^{(n)2} (\Phi_{\mu\nu}^{(n)} \Xi_{\mu\nu}^{(n)} \mu - \tilde{\Phi}_{\mu\nu}^{(n)} \tilde{\Xi}_{\mu\nu}^{(n)} \nu), \quad (\text{C41})$$

$$C_{\mu\nu}^{(n)} = i v_{gf}^{(n)4} v_{ge}^{(n)2} (\Phi_{\mu\nu}^{(n)} \Xi_{\mu\nu}^{(n)2} \mu - \tilde{\Phi}_{\mu\nu}^{(n)} \tilde{\Xi}_{\mu\nu}^{(n)2} \nu) - i v_{gf}^{(n)2} [\Xi_{\mu\nu}^{(n)} (\tilde{\omega}_{ef}^{(n)} + \tilde{\omega}_{\mu-1\nu}) - \tilde{\Xi}_{\mu\nu}^{(n)} (\tilde{\omega}_{ef}^{(n)*} - \tilde{\omega}_{\mu\nu-1})], \quad (\text{C42})$$

$$E_{\mu\nu}^{(n)} = i v_{ge}^{(n)2} \sqrt{\mu\nu} (\Phi_{\mu\nu}^{(n)} - \tilde{\Phi}_{\mu\nu}^{(n)}), \quad (\text{C43})$$

$$F_{\mu\nu}^{(n)} = i v_{ge}^{(n)2} v_{gf}^{(n)2} \sqrt{\mu\nu} (\Phi_{\mu\nu}^{(n)} \Xi_{\mu\nu}^{(n)} - \tilde{\Phi}_{\mu\nu}^{(n)} \tilde{\Xi}_{\mu\nu}^{(n)}), \quad (\text{C44})$$

$$G_{\mu\nu}^{(n)} = i v_{ge}^{(n)2} (\tilde{\Phi}_{\mu\nu}^{(n)} \mu - \Phi_{\mu\nu}^{(n)} \nu). \quad (\text{C45})$$

In the next step, we calculate the inverse matrix of $M_{n;\mu\nu}^{(ij)}$ and denote it as $O_{n;\mu\nu}^{(ij)}$ to solve Eq. (C30):

$$\rho_{g\mu,gv}^{(n)} = (O_{n;\mu\nu}^{(11)} k_{e \rightarrow g}^{(n)} - O_{n;\mu\nu}^{(12)} k_{e \rightarrow f}^{(n)}) \rho_{\mu\nu} - O_{n;\mu\nu}^{(13)} k_{f \rightarrow e}^{(n)} \rho_{\mu-1\nu-1}, \quad (\text{C46})$$

$$\rho_{e\mu-1,ev-1}^{(n)} = (O_{n;\mu\nu}^{(21)} k_{e \rightarrow g}^{(n)} - O_{n;\mu\nu}^{(22)} k_{e \rightarrow f}^{(n)}) \rho_{\mu\nu} - O_{n;\mu\nu}^{(23)} k_{f \rightarrow e}^{(n)} \rho_{\mu-1\nu-1}, \quad (\text{C47})$$

$$\rho_{f\mu,fv}^{(n)} = (O_{n;\mu\nu}^{(31)} k_{e \rightarrow g}^{(n)} - O_{n;\mu\nu}^{(32)} k_{e \rightarrow f}^{(n)}) \rho_{\mu\nu} - O_{n;\mu\nu}^{(33)} k_{f \rightarrow e}^{(n)} \rho_{\mu-1\nu-1}. \quad (\text{C48})$$

Inserting Eqs. (C46)–(C48) into Eqs. (C26) and (C27), we get

$$\begin{aligned} \rho_{g\mu,gv}^{(n)} &= \tilde{\Phi}_{\mu\nu}^{(n)} \tilde{\Xi}_{\mu\nu}^{(n)} v_{gf}^{(n)2} v_{ge}^{(n)2} \sqrt{\nu} [(O_{n;\mu\nu}^{(11)} - O_{n;\mu\nu}^{(31)}) k_{e \rightarrow g}^{(n)} - (O_{n;\mu\nu}^{(12)} - O_{n;\mu\nu}^{(32)}) k_{e \rightarrow f}^{(n)}] \rho_{\mu\nu} \\ &\quad - \tilde{\Phi}_{\mu\nu}^{(n)} \tilde{\Xi}_{\mu\nu}^{(n)} v_{gf}^{(n)2} v_{ge}^{(n)2} \sqrt{\nu} (O_{n;\mu\nu}^{(13)} - O_{n;\mu\nu}^{(33)}) k_{f \rightarrow e}^{(n)} \rho_{\mu-1\nu-1} + \tilde{\Phi}_{\mu\nu}^{(n)} v_{ge}^{(n)} [(\sqrt{\nu} O_{n;\mu\nu}^{(11)} - \sqrt{\mu} O_{n;\mu\nu}^{(21)}) k_{e \rightarrow g}^{(n)} \\ &\quad - (\sqrt{\nu} O_{n;\mu\nu}^{(12)} - \sqrt{\mu} O_{n;\mu\nu}^{(22)}) k_{e \rightarrow f}^{(n)}] \rho_{\mu\nu} - \tilde{\Phi}_{\mu\nu}^{(n)} v_{ge}^{(n)} (\sqrt{\nu} O_{n;\mu\nu}^{(13)} - \sqrt{\mu} O_{n;\mu\nu}^{(23)}) k_{f \rightarrow e}^{(n)} \rho_{\mu-1\nu-1}. \end{aligned} \quad (\text{C49})$$

$$\begin{aligned} \rho_{e\mu-1,gv}^{(n)} &= \Phi_{\mu\nu}^{(n)} \Xi_{\mu\nu}^{(n)} v_{gf}^{(n)2} v_{ge}^{(n)2} \sqrt{\mu} [(O_{n;\mu\nu}^{(11)} - O_{n;\mu\nu}^{(31)}) k_{e \rightarrow g}^{(n)} - (O_{n;\mu\nu}^{(12)} - O_{n;\mu\nu}^{(32)}) k_{e \rightarrow f}^{(n)}] \rho_{\mu\nu} \\ &\quad - \Phi_{\mu\nu}^{(n)} \Xi_{\mu\nu}^{(n)} v_{gf}^{(n)2} v_{ge}^{(n)2} \sqrt{\mu} (O_{n;\mu\nu}^{(13)} - O_{n;\mu\nu}^{(33)}) k_{f \rightarrow e}^{(n)} \rho_{\mu-1\nu-1} + \Phi_{\mu\nu}^{(n)} v_{ge}^{(n)} [(\sqrt{\mu} O_{n;\mu\nu}^{(11)} - \sqrt{\nu} O_{n;\mu\nu}^{(21)}) k_{e \rightarrow g}^{(n)} \\ &\quad - (\sqrt{\mu} O_{n;\mu\nu}^{(12)} - \sqrt{\nu} O_{n;\mu\nu}^{(22)}) k_{e \rightarrow f}^{(n)}] \rho_{\mu\nu} - \Phi_{\mu\nu}^{(n)} v_{ge}^{(n)} (\sqrt{\mu} O_{n;\mu\nu}^{(13)} - \sqrt{\nu} O_{n;\mu\nu}^{(23)}) k_{f \rightarrow e}^{(n)} \rho_{\mu-1\nu-1}. \end{aligned} \quad (\text{C50})$$

With these results, we are now ready to consider the following summations

$$i v_{ge}^{(n)} (\sqrt{\mu} \rho_{e\mu-1,gv}^{(n)} - \sqrt{\nu} \rho_{g\mu,gv}^{(n)}) = H_{\mu\nu}^{(n)} \rho_{\mu\nu} - I_{\mu\nu}^{(n)} \rho_{\mu-1\nu-1}, \quad (\text{C51})$$

$$i v_{ge}^{(n)} (\sqrt{\nu} \rho_{e\mu-1,gv}^{(n)} - \sqrt{\mu} \rho_{g\mu,gv}^{(n)}) = J_{\mu\nu}^{(n)} \rho_{\mu\nu} - K_{\mu\nu}^{(n)} \rho_{\mu-1\nu-1}. \quad (\text{C52})$$

Here, we have introduced the following abbreviations

$$H_{\mu\nu}^{(n)} = [(A_{\mu\nu}^{(n)} + B_{\mu\nu}^{(n)}) O_{n;\mu\nu}^{(11)} - E_{\mu\nu}^{(n)} O_{n;\mu\nu}^{(21)} - B_{\mu\nu}^{(n)} O_{n;\mu\nu}^{(31)}) k_{e \rightarrow g}^{(n)} - [(A_{\mu\nu}^{(n)} + B_{\mu\nu}^{(n)}) O_{n;\mu\nu}^{(12)} - E_{\mu\nu}^{(n)} O_{n;\mu\nu}^{(22)} - B_{\mu\nu}^{(n)} O_{n;\mu\nu}^{(32)}) k_{e \rightarrow f}^{(n)}, \quad (\text{C53})$$

$$I_{\mu\nu}^{(n)} = [(A_{\mu\nu}^{(n)} + B_{\mu\nu}^{(n)}) O_{n;\mu\nu}^{(13)} - E_{\mu\nu}^{(n)} O_{n;\mu\nu}^{(23)} - B_{\mu\nu}^{(n)} O_{n;\mu\nu}^{(33)}) k_{f \rightarrow e}^{(n)}, \quad (\text{C54})$$

$$\begin{aligned} J_{\mu\nu}^{(n)} &= [(E_{\mu\nu}^{(n)} + F_{\mu\nu}^{(n)}) O_{n;\mu\nu}^{(11)} + G_{\mu\nu}^{(n)} O_{n;\mu\nu}^{(21)} - F_{\mu\nu}^{(n)} O_{n;\mu\nu}^{(31)}) k_{e \rightarrow g}^{(n)} \\ &\quad - [(E_{\mu\nu}^{(n)} + F_{\mu\nu}^{(n)}) O_{n;\mu\nu}^{(12)} + G_{\mu\nu}^{(n)} O_{n;\mu\nu}^{(22)} - F_{\mu\nu}^{(n)} O_{n;\mu\nu}^{(32)}) k_{e \rightarrow f}^{(n)}, \end{aligned} \quad (\text{C55})$$

$$K_{\mu\nu}^{(n)} = [(E_{\mu\nu}^{(n)} + F_{\mu\nu}^{(n)}) O_{n;\mu\nu}^{(13)} + G_{\mu\nu}^{(n)} O_{n;\mu\nu}^{(23)} - F_{\mu\nu}^{(n)} O_{n;\mu\nu}^{(33)}) k_{f \rightarrow e}^{(n)}. \quad (\text{C56})$$

Inserting Eqs. (C51) and (C52) into Eq. (C1), we get the equations for the plasmon RDM only:

$$\begin{aligned} \frac{\partial}{\partial t} \rho_{\mu\nu} &= -i \omega_{\mu\nu} \rho_{\mu\nu} - \gamma_{\text{pl}} [(\mu + \nu)/2] \rho_{\mu\nu} + \gamma_{\text{pl}} \sqrt{(\mu + 1)(\nu + 1)} \rho_{\mu+1\nu+1} \\ &\quad - \sum_{n=1}^{N_m} (H_{\mu\nu}^{(n)} + K_{\mu+1\nu+1}^{(n)}) \rho_{\mu\nu} + \sum_{n=1}^{N_m} I_{\mu\nu}^{(n)} \rho_{\mu-1\nu-1} + \sum_{n=1}^{N_m} J_{\mu+1\nu+1}^{(n)} \rho_{\mu+1\nu+1}. \end{aligned} \quad (\text{C57})$$

The diagonal element of the plasmon RDM can be interpreted as the plasmon state population $P_\mu = \rho_{\mu\mu}$. The equations for the population can be easily achieved from Eq. (C57) and are given as Eq. (3) in the main text. There, we have introduced the

molecule-induced plasmon damping rate

$$k_{\mu} = \sum_{n=1}^{N_m} H_{\mu\mu}^{(n)} = \sum_{n=1}^{N_m} J_{\mu\mu}^{(n)}, \quad (\text{C58})$$

and the molecule-induced plasmon pumping rate

$$p_{\mu} = \sum_{n=1}^{N_m} I_{\mu\mu}^{(n)} = \sum_{n=1}^{N_m} K_{\mu\mu}^{(n)}. \quad (\text{C59})$$

-
- [1] M. S. Tame, K. R. McEnergy, Ş. K. Özdemir, J. Lee, S. A. Maier, and M. S. Kim, *Nat. Phys.* **9**, 329 (2013).
- [2] R. M. Ma, R. F. Oulton, V. J. Sorger, and X. Zhang, *Laser Photon. Rev.* **7**, 1 (2013).
- [3] M. Pelton, J. Aizpurua, and G. Bryant, *Laser & Photon. Rev.* **2**, 136 (2008).
- [4] P. Berini and I. D. Leon, *Nat. Photon.* **6**, 16 (2012).
- [5] N. I. Cade, T. Ritman-Meer, and D. Richards, *Phys. Rev. B* **79**, 241404 (2009).
- [6] Y. Zelinskyy, Y. Zhang, and V. May, *J. Phys. Chem. A* **116**, 11330 (2012).
- [7] P. Anger, P. Bharadwaj, and L. Novotny, *Phys. Rev. Lett.* **96**, 113002 (2006).
- [8] M. Fleischmann, P. J. Hendra, and A. J. McQuillan, *Chem. Phys. Lett.* **26**, 163 (1947).
- [9] P. Johansson, H. X. Xu, and M. Käll, *Phys. Rev. B* **72**, 035427 (2005).
- [10] S. Y. Ding, X. M. Zhang, B. Ren, and Z. Q. Tian, *Surface-Enhanced Raman Spectroscopy: General Introduction*, Encyclopedia of Analytical Chemistry (Wiley, New York, 2014).
- [11] S. Nie and S. R. Emory, *Science* **275**, 1102 (1997).
- [12] X. F. Gu, T. Qiu, W. J. Zhang, and P. K. Chu, *Nano. Res. Lett.* **6**, 199 (2011).
- [13] N. Gao, K. Huang, J. C. Li, S. P. Li, X. Yang, and J. Y. Kang, *Sci. Rep.* **2**, 816 (2012).
- [14] H. A. Atwater and A. Polman, *Nat. Mater.* **9**, 205 (2010).
- [15] J. L. Wu, F. C. Chen, Y. S. Hsiao, F. C. Chien, P. Chen, C. H. Kuo, M. H. Huang, and C. S. Hsu, *ACS Nano* **5**, 959 (2011).
- [16] D. J. Bergman and M. I. Stockman, *Phys. Rev. Lett.* **90**, 027402 (2003).
- [17] M. A. Noginov, G. Zhu, A. M. Belgrave, R. Bakker, V. M. Shalaev, E. E. Narimanov, S. Stout, E. Herz, T. Suteewong, and U. Wiesner, *Nature* **460**, 1110 (2009).
- [18] J. Ho, J. Tatebayashi, S. Sergent, C. F. Fong, Y. Ota, S. Iwamoto, and Y. Arakawa, *ACS Photon.* **2**, 165 (2015).
- [19] Y. H. Chou, B. T. Chou, C. K. Chiang, Y. Y. Lai, C. T. Yang, H. Li, T. R. Lin, C. C. Lin, H. C. Kuo, S. C. Wang, and T. C. Lu, *ACS Nano* **9**, 3978 (2015).
- [20] B. T. Chou, Y. H. Chou, Y. M. Wu, Y. C. Chung, W. J. Hsueh, S. W. Lin, T. C. Lu, T. R. Lin, and S. D. Lin, *Sci. Rep.* **6**, 19887 (2016).
- [21] R. M. Ma, R. F. Oulton, V. J. Sorger, G. Bartal, and X. Zhang, *Nat. Mater.* **10**, 110 (2011).
- [22] R. M. Ma, X. B. Yin, R. F. Oulton, V. J. Sorger, and X. Zhang, *Nano. Lett.* **12**, 5396 (2012).
- [23] M. Khajavikhan, A. Simic, M. Katz, J. H. Lee, B. Slutsky, A. Mizrahi, V. Lomakin, and Y. Fainman, *Nature* **482**, 204 (2012).
- [24] K. Ding, Z. C. Liu, L. J. Yin, M. T. Hill, M. J. H. Marell, P. J. van Veldhoven, R. Noetzel, and C. Z. Ning, *Phys. Rev. B* **85**, 041301(R) (2012).
- [25] A. Matsudaira, C. Y. Lu, M. Zhang, S. L. Chuang, and D. Bimberg, *IEEE Photon.* **4**, 1103 (2012).
- [26] C. Y. Lu, C. Y. Ni, M. Zhang, S. L. Chuang, and D. H. Bimberg, *IEEE J. Quantum Electron.* **19**, 1 (2013).
- [27] C. Y. Lu, S. L. Chuang, and D. Bimberg, *IEEE J. Quantum Electron.* **49**, 114 (2013).
- [28] S. W. Chang, C. Y. Lu, S. L. Chuang, T. D. German, U. W. Pohl, and D. Bimberg, *IEEE J. Quantum Electron.* **17**, 1681 (2011).
- [29] J. Y. Suh, C. H. Kim, W. Zhou, M. D. Huntington, D. T. Co, M. R. Wasielewski, and T. W. Odom, *Nano Lett.* **12**, 5769 (2012).
- [30] W. Zhou, M. Dridi, J. Y. Suh, C. H. Kim, D. T. Co, M. R. Wasielewski, G. C. Schatz, and T. W. Odom, *Nat. Nanotech.* **8**, 506 (2013).
- [31] A. Yang, T. B. Hoang, M. Dridi, C. Deeb, M. H. Mikkelsen, G. C. Schatz, and T. W. Odom, *Nat. Commun.* **6**, 6939 (2015).
- [32] A. Yang, Z. Y. Li, M. P. Knudson, A. J. Hryn, W. J. Wang, K. Aydin, and T. W. Odom, *ACS. Nano.* **9**, 11582 (2015).
- [33] A. H. Schokker and A. F. Koenderink, *ACS Photon.* **2**, 1289 (2015).
- [34] M. Richter, M. Gegg, T. S. Theuerholz, and A. Knorr, *Phys. Rev. B* **91**, 035306 (2015).
- [35] V. M. Parfenyev and S. S. Vergeles, *Opt. Express* **22**, 13671 (2014).
- [36] M. Sargent II, M. O. Scully, and W. E. Lamb, *Laser Physics* (Addison-Wesley, Reading, MA, 1974).
- [37] K. J. Savage, M. M. Hawkeye, R. Esteban, A. G. Borisov, J. Aizpurua, and J. J. Baumberg, *Nature* **491**, 574 (2012).
- [38] Y. Zhang and K. Mølmer, *J. Phys. Chem. C* **121**, 15339 (2017).
- [39] Y. Zhang and V. May, *Phys. Rev. B* **89**, 245441 (2014).
- [40] J. Gersten and A. Nitzan, *J. Chem. Phys.* **75**, 1139 (1981).
- [41] G. V. Hartland, *Chem. Rev.* **111**, 3858 (2011).
- [42] U. Martini, Ph.D. thesis, Ludwig-Maximilians-University, 2000.
- [43] B. A. Chase and J. M. Geremia, *Phys. Rev. A* **78**, 052101 (2008).
- [44] M. Xu, D. A. Tieri, and M. J. Holland, *Phys. Rev. A* **87**, 062101 (2013).
- [45] Y. Zhang and V. May, *J. Chem. Phys.* **142**, 224702 (2015).
- [46] M. Gegg and M. Richter, *New J. Phys.* **18**, 043037 (2016).
- [47] Y. Zhang, K. Mølmer, and V. May, *Phys. Rev. B* **94**, 045412 (2016).
- [48] Y. Zhang and K. Mølmer (unpublished).
- [49] P. Meystre and M. Sargent, *Elements of Quantum Optics* (Springer-Verlag, Berlin, 1990).
- [50] J. Mompert and R. Corbalan, *J. Opt. B.: Quantum Semiclass. Opt.* **2**, R7 (2000).
- [51] M. O. Scully and M. S. Zubairy, *Quantum Optics* (Cambridge University, Cambridge, England, 2001).